

Large Eddy Simulation of Flow over a Cylinder Using High-Order Spectral Difference Method

Abrar H. Mohammad* and Z. J. Wang†
Iowa State University, Ames, IA 50011, U.S.A.

Chunlei Liang‡
Stanford University, Stanford, CA 94305, U.S.A.

Large eddy simulation of the flow over a circular cylinder at Reynolds number $Re_D = 2580$ has been studied with a high-order unstructured spectral difference method. Grid and accuracy refinement studies were carried out to assess numerical errors. The mean and fluctuating velocity fields in the wake of a circular cylinder were compared with PIV experimental measurements. The numerical results are in an excellent agreement with the measurements for both the mean velocity and Reynolds stresses. Other wake characteristics such as the recirculation bubble length, vortex formation length and maximum intensity of the velocity fluctuations have also been predicted accurately. The numerical simulations demonstrated the potential of the high-order SD method in large eddy simulation of physically complex problems.

Keywords: LES, spectral difference, circular cylinder, coherent structures, vortex shedding, bluff body

I. Introduction

The flow around bluff bodies is very complex and can involve regions of laminar, transitional and turbulent flows, unsteady separation and reattachment, and the formation of coherent structures, particularly in the wake region of the flow. The understanding of bluff body vortex shedding is of great practical importance and the uniform flow over a circular cylinder is a classical example of bluff body flow. The configuration is quite simple but the flow is characterized by a very complex wake at Reynolds number $Re_D=2580$ examined in this paper. In this paper, we try to show the importance of using high order methods to study the numerical and physical aspect of unsteady wake flow involving separation, recirculation, unsteady vortex shedding and large complex flow structures at a sub-critical Reynolds number. The near wake structure behind a bluff body plays an important role in the overall vortex formation and shedding processes and determines the magnitude of mean and fluctuating forces exerted on the body. Direct numerical simulations (DNS) of the Navier-Stokes equations, in which all eddy scales have to be captured, is almost impossible for problems with moderately high Reynolds number because of the huge computational requirements in resolving all turbulence scales. Hence a less expensive and accurate method is required. In Reynolds averaged Navier-Stokes (RANS) approach, all eddies are averaged over to give equations for variables representing the mean flow. But RANS has proved to be generally inadequate in predicting the effects of turbulent separating and reattaching flows, because the large eddies responsible for the primary transport are geometry dependent. For any turbulent flow, the largest scale is of the order of the domain size and the small scales are related to the dissipative eddies where the viscous effects become predominant. Large eddy simulation (LES) is a method where the three-dimensional and unsteady motion of the large eddies is computed explicitly and the non-linear interactions with the smaller eddies, which are assumed to be isotropic and universal, are modeled. LES is an active area of research and the numerical simulation of complex flows is essential in the development of the method as a tool to predict flows of engineering interest.

In this paper, implicit LES computations were performed without any sub-grid scale model in order to investigate the effectiveness of the spectral difference method. These simulations were deliberately not called direct numerical simulations because they did not comply with the resolution requirements of DNS. Turbulent flow past a circular cylinder has been the subject of a large number of experimental and numerical investigations^{1,2}. In recent years a good understanding of the physics of flow at low Reynolds number of below a few hundred, has been

* Graduate Research Assistant, Department of Aerospace Engineering, abrar@iastate.edu.

† Professor of Aerospace Engineering, 2271 Howe Hall, zjw@iastate.edu, Associate Fellow of AIAA

‡ Research Associate, Department of Aeronautics and Astronautics, chliang@stanford.edu, AIAA Member.

obtained. But at higher Reynolds number, still subcritical though, considerably less is known. A comprehensive review of the flow characteristics for a wide range of Reynolds numbers was studied by Williamson³. In addition, a number of simulations at various Reynolds numbers, mostly LES, have been carried out^{4,5}. The cylinder flow at Reynolds number $Re_D=3900$ has become a common test case for LES primarily because of the availability of the experimental results of Lourenco and Shih⁶ and Ong and Wallace⁷. The calculations were performed on structured⁸⁻¹¹ and unstructured meshes¹²⁻¹⁴. Beaudan and Moin⁹, Mittal and Moin¹⁰, Kravchenko and Moin¹⁵ were among the first to perform LES studies at $Re_D=3900$. Motivated by the direct simulation results of Rai and Moin¹⁶, Beaudan and Moin⁹ used high-order upwind-biased schemes for the numerical simulations of the compressible Navier–Stokes equations. The profiles of mean velocity and Reynolds stresses obtained in these simulations were in reasonable agreement with the experimental data. However, inside the recirculation region, the streamwise velocity profiles differed in shape from those observed in the experiment⁶. These differences were attributed to the experimental errors as manifested in the large asymmetry of the experimental data⁹. A new experiment at the same Reynolds number was carried out by Ong and Wallace⁷ and provided the mean flow data at several locations in the near wake of the cylinder downstream of the recirculation region. Even though fair agreement between the simulations of Beaudan and Moin⁹ and the experiment was observed in the mean velocity profiles, turbulence intensities at several downstream locations did not match the experimental data. Also the Reynolds stresses were not predicted correctly when compared to experimental data. Similar problems were observed with Mittal and Moin's work^{10,11}. In the two mentioned simulations, they showed a shape of the streamwise velocity profile inside the recirculation region different from that observed in the experiment of Lourenco and Shih⁶. A new experiment at the same Reynolds number was carried out by Ong and Wallace⁷ and provided the mean flow data at several locations in the near wake of the cylinder downstream of the recirculation region. Even though fair agreement between the simulations of Beaudan and Moin⁹ and the experiment was observed in the mean velocity profiles, turbulence intensities at several downstream locations did not match the experimental data. Several other researchers have examined a variety of aspects that affect the quality of LES solutions at $Re_D=3900$. The numerical and modeling aspects which influence the quality of LES solutions were studied by Breuer¹⁷. He had also carried out LES computations without any sub-grid scale model.

DNS of the cylinder flow at $Re_D=3900$ was performed by Ma *et al.*¹³. The mean velocity profiles and the power spectra are in good agreement with the experimental data in the near wake as well as far downstream. In particular, the velocity profiles agree well with those from the experiments in the vicinity of the cylinder. Compared with LES¹¹, the pressure coefficient in DNS is a little lower, while the recirculation bubble length is larger. Franke and Frank¹⁸ found out that this is an effect of the averaging time in computing statistics. In DNS¹³ the statistics is accumulated over 600 convective time units (D/U), while in LES¹¹ the statistics is accumulated over 35 convective time units. The numerical issues raised in the previous large eddy simulations prompted us to attempt simulations of the flow over a circular cylinder using a high order method. Second-order simulations for unperturbed inlet flow conditions at $Re_D=2580$ were performed by Liang¹⁹. The length of the recirculation bubble was under predicted probably due to under-resolution. The primary motivation for using a high order method is to accurately study the wake flow at Reynolds number $Re_D=2580$. The numerical results obtained were compared with the PIV experiment performed by Konstantinidis *et al.*²⁰.

II. Numerical Approach: The Spectral Difference Method

High-order methods capable of handling unstructured grids are highly sought after in many practical applications with complex geometries in LES, DNS of turbulence, computational aero-acoustics, to name a few. The spectral difference (SD) method²¹⁻²⁴ is a high order, conservative and efficient method for conservation laws on unstructured grids^{8,21}. The SD method is similar to the finite-difference method and it utilizes the concept of discontinuous and high order local representations to achieve conservation and high accuracy in a manner similar to discontinuous Galerkin (DG) method²⁵⁻²⁶ or spectral volume (SV) method²⁷⁻³⁰. For quadrilateral and hexahedral grids, the SD method^{31,32} is identical to the staggered-grid multi-domain spectral method³³. The method is very simple to implement since it involves one-dimensional operations only, and does not involve any surface or volume integrals. The SD method is based on the differential form. The basic idea is presented next for the Navier-Stokes equations.

Consider the unsteady compressible 3D Navier-Stokes equations in conservative form written as

$$\frac{\partial Q}{\partial t} + \frac{\partial F}{\partial x} + \frac{\partial G}{\partial y} + \frac{\partial H}{\partial z} = 0, \quad (1)$$

where Q is the vector of conserved variables, and F, G, H are the total fluxes including both the inviscid and viscous flux vectors, i.e., $F = F^i - F^v$, $G = G^i - G^v$, $H = H^i - H^v$.

We employ non-overlapping unstructured hexahedral cells or elements to fill the computational domain. In order to handle curved boundaries, both linear and quadratic iso-parametric elements are employed, with linear elements used in the interior domain and quadratic elements near high-order curved boundaries. In order to achieve an efficient implementation, all elements are transformed from the physical domain (x, y, z) into a standard element $(\xi, \eta, \zeta) \in [0, 1] \times [0, 1] \times [0, 1]$. The governing equations in the physical domain are then transformed into the computational domain (standard element), and the transformed equations take the following form

$$\frac{\partial \tilde{Q}}{\partial t} + \frac{\partial \tilde{F}}{\partial \xi} + \frac{\partial \tilde{G}}{\partial \eta} + \frac{\partial \tilde{H}}{\partial \zeta} = 0. \quad (2)$$

In the standard element, two sets of points are defined, namely the solution points and the flux points. The solution unknowns or degrees-of-freedom (DOFs) are the conserved variables at the solution points, while fluxes are computed at the flux points. In order to construct a degree $(N-1)$ polynomial in each coordinate direction, solutions at N points are required. In a recent study, Van den Abeele *et al*³⁴ found that the SD method does not depend on where the solution points are located, while the location of the flux points determines the method. Therefore, the solution points can be chosen to maximize efficiency. It was also found that the use of Chebyshev-Gauss-Lobatto points as the flux points results in a weak instability by Van den Abeele *et al*³⁴ and Huynh³⁵. In the present simulation, the solution points are chosen to be the Chebyshev-Gauss points defined by

$$X_s = \frac{1}{2} \left[1 - \cos \left(\frac{2s-1}{2N} \cdot \pi \right) \right], \quad s = 1, 2, \dots, N. \quad (3)$$

The flux points are selected to be the Legendre-Gauss-quadrature points plus the two end points, 0 and 1, as suggested by Huynh³⁵. Using the N solutions at the solution points, a degree $N-1$ polynomial can be built using the following Lagrange basis defined as

$$h_i(X) = \prod_{s=1, s \neq i}^N \left(\frac{X - X_s}{X_i - X_s} \right). \quad (4a)$$

Similarly, using the $N+1$ fluxes at the flux points, a degree N polynomial can be built for the flux using a similar Lagrange basis defined as

$$l_{i+1/2}(X) = \prod_{s=0, s \neq i}^N \left(\frac{X - X_{s+1/2}}{X_{i+1/2} - X_{s+1/2}} \right). \quad (4b)$$

The reconstructed solution for the conserved variables in the standard element is just the tensor products of the three one-dimensional polynomials, i.e.,

$$Q(\xi, \eta, \zeta) = \sum_{k=1}^N \sum_{j=1}^N \sum_{i=1}^N \frac{\tilde{Q}_{i,j,k}}{J_{i,j,k}} h_i(\xi) \cdot h_j(\eta) \cdot h_k(\zeta). \quad (5)$$

Similarly, the reconstructed flux polynomials take the following forms:

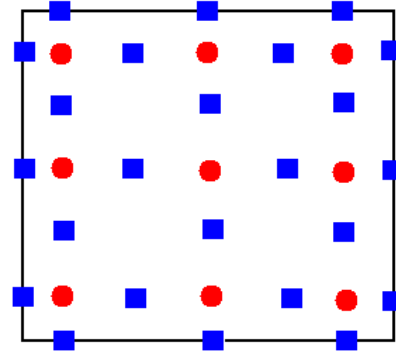


Fig. 1. Distribution of solution points (circles) and flux points (squares) in a standard element for a 3rd order SD scheme.

$$\tilde{F}(\xi, \eta, \varsigma) = \sum_{k=1}^N \sum_{j=1}^N \sum_{i=0}^N \tilde{F}_{i+1/2, j, k} l_{i+1/2}(\xi) \cdot h_j(\eta) \cdot h_k(\varsigma), \quad (6a)$$

$$\tilde{G}(\xi, \eta, \varsigma) = \sum_{k=1}^N \sum_{j=0}^N \sum_{i=1}^N \tilde{G}_{i, j+1/2, k} h_i(\xi) \cdot l_{j+1/2}(\eta) \cdot h_k(\varsigma), \quad (6b)$$

$$\tilde{H}(\xi, \eta, \varsigma) = \sum_{k=0}^N \sum_{j=1}^N \sum_{i=1}^N \tilde{H}_{i, j, k+1/2} h_i(\xi) \cdot h_j(\eta) \cdot l_{k+1/2}(\varsigma). \quad (6c)$$

The reconstructed fluxes are only element-wise continuous, but discontinuous across cell interfaces. For the inviscid flux, a Riemann solver, such as the Rusanov or Roe flux, is employed to compute a common flux at interfaces to ensure conservation and stability. In summary, the algorithm to compute the inviscid flux derivatives consists of the following steps:

1. Given the conserved variables at the solution points $\{\tilde{Q}_{i,j,k}\}$, compute the conserved variables at the flux points
2. Compute the inviscid fluxes at the interior flux points using the solutions computed at Step 1
3. Compute the inviscid flux at element interfaces using a Riemann solver, in terms of the left and right conserved variables of the interface.
4. Compute the derivatives of the fluxes at all the solution points according to

$$\left(\frac{\partial \tilde{F}}{\partial \xi} \right)_{i,j,k} = \sum_{r=0}^N \tilde{F}_{r+1/2, j, k} \cdot l'_{r+1/2}(\xi_i), \quad (7a)$$

$$\left(\frac{\partial \tilde{G}}{\partial \eta} \right)_{i,j,k} = \sum_{r=0}^N \tilde{G}_{i, r+1/2, k} \cdot l'_{r+1/2}(\eta_j), \quad (7b)$$

$$\left(\frac{\partial \tilde{H}}{\partial \varsigma} \right)_{i,j,k} = \sum_{r=0}^N \tilde{H}_{i, j, r+1/2} \cdot l'_{r+1/2}(\varsigma_k). \quad (7c)$$

The viscous flux is a function of both the conserved variables and their gradients, e.g., $\tilde{F}_{i+1/2, j, k}^v = \tilde{F}^v(Q_{i+1/2, j, k}, \nabla Q_{i+1/2, j, k})$. Therefore the key is how to compute the solution gradients at the flux points. The following steps are taken to compute the viscous fluxes:

1. Same as Step 1 for the inviscid flux computations;
2. When computing the derivatives, the solution Q at the cell interface is not uniquely defined. The solution at the interface is simply the average of the left and right solutions, $\hat{Q} = (Q_L + Q_R)/2$.
3. Compute the gradients of the solution at the solution points using the solutions at the flux points. Then the gradients are interpolated from the solution points to the flux points using the same Lagrangian interpolation approach given in.
4. Compute the viscous flux at the flux points using the solutions and their gradients at the flux points. Again at cell interfaces, the gradients have two values, one from the left and one from the right. The gradients used in the viscous fluxes at the cell interface are simply the averaged ones, i.e., $\tilde{F}^v = \tilde{F}^v((Q_L + Q_R)/2, (\nabla Q_L + \nabla Q_R)/2)$.

More details of the SD method can be found in References 31 and 32.

III. Problem Definition and Computational Details

The simulation was performed to match the geometry of the experiment performed by Konstantinidis *et al*²⁰. The experiments were performed using the PIV technique in a stainless steel water tunnel with a cross-section of 72mm x 72mm. The origin and size of the computational domain are shown in Fig 2. The x-axis is along the streamwise flow direction and the z-axis is along the cylinder axis i.e. the spanwise direction. The cylinder has a

non-dimensional unit diameter. The upstream velocity is fixed at $U=0.1$ m/s and is assumed to be uniform across the inlet. The Reynolds number based on the cylinder diameter and upstream velocity is 2580.

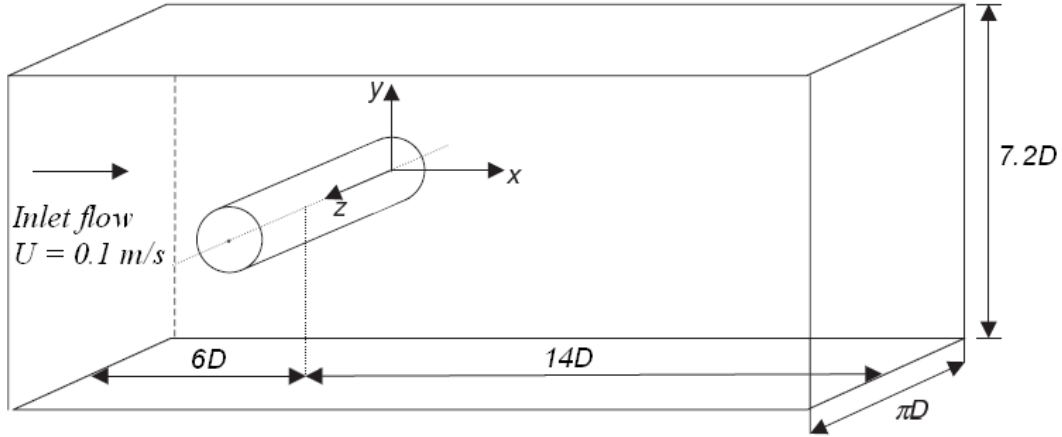


Fig. 2. The geometry of the flow over cylinder

The size of the computational domain in the y -direction is equal to 7.2 cylinder diameters, which is equal to the one used in the experiment. The required size in the spanwise direction is estimated from the prior knowledge of the sizes of the streamwise vortex structures. It has been reported in the experimental studies by Mansy *et al.*³⁶ and Williamson *et al.*³⁷ that the wavelength of the streamwise structures in the near wake of a circular cylinder scale as

$$\lambda_z/D \sim 25 \text{Re}_D^{-0.5} \quad (8)$$

For the present case of $\text{Re}_D=2580$, the wavelength is approximately $0.5D$. Further downstream, large scale structures were observed by Williamson *et al.*³⁷ with wavelengths $\lambda_z/D \sim 1$. No experimental information was available about the size of streamwise structures, so the length of the domain in the spanwise direction is taken to be πD which is the same as the one used by Kravchenko and Moin¹¹, and Breuer⁸.

High-order spectral difference method is employed to solve the problem. Implicit scheme with 2nd order accuracy in time was used. Both 2nd and 3rd orders of spatial accuracy were tested with quadratic boundary for the cylinder surface. Although the explicit scheme is easy to implement and has high-order accuracy in time, it suffered from too small time step, especially for viscous grids which are clustered in the viscous boundary layer. It is well-known that high-order methods are restricted to a smaller CFL number than low order ones. In addition, they also possess much less numerical dissipation. The computation cost of high-order explicit methods for many steady-state problems is so high that they become less efficient than low-order implicit methods in terms of the total CPU time given the same level of solution error. Therefore an efficient implicit lower-upper symmetric Gauss-Seidel (LU-SGS)^{38,39} solution algorithm is used to solve viscous compressible flows for the high order spectral difference method on unstructured hexahedral grids.

As shown in Fig. 3 and Fig. 4, two meshes are used. The coarse mesh has 86,680 cells and the fine mesh has 189,448 cells. For third order spatial accuracy, the coarse mesh has 2.34 million degrees-of-freedom (DOFs) while the fine mesh has 5.12 million DOFs. The fine mesh is produced by refining the coarse mesh by about 1.5 times in the wake region of the cylinder.

As mentioned earlier, the length of the domain in the spanwise direction is πD and 12 layers are used for coarse mesh while 18 layers are used for the fine mesh. A constant expansion of 1.1 was used in the radial direction away from the cylinder. The smallest cell spacing in the radial direction is $\Delta r_{\min}/D = 1.75 \times 10^{-3}$ for the fine mesh and 3.5×10^{-3} for the coarse mesh. Beaudan and Moin⁹ had used a slightly lower value of $\Delta r_{\min}/D = 1.25 \times 10^{-3}$ for their finest mesh at $\text{Re}_D=3900$. Therefore the mesh used in this paper is coarser than the finest mesh used by Beaudan and Moin⁹. In every layer in the spanwise direction, 120 cells were placed along the circumference of the cylinder for coarse mesh while 160 for fine mesh which is lower than the ones used by Liang¹⁹ at $\text{Re}_D=2580$.

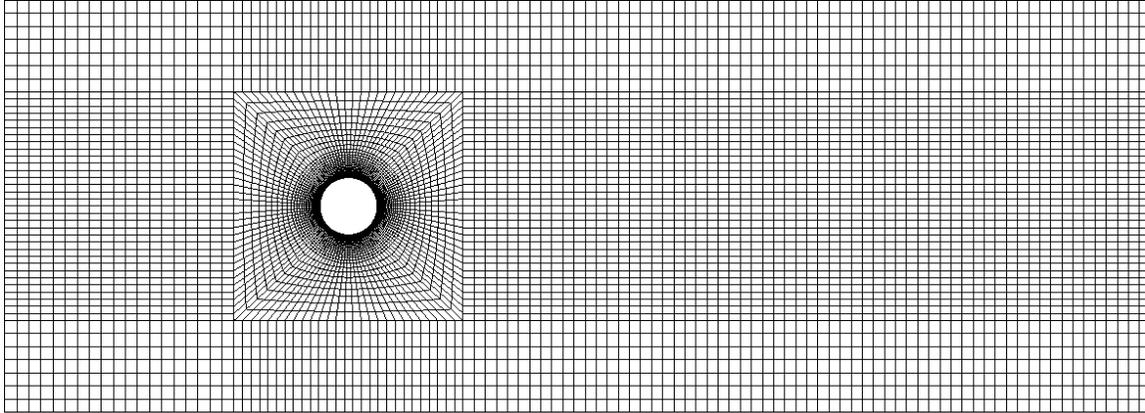


Fig. 3. Coarse mesh in X-Y plane

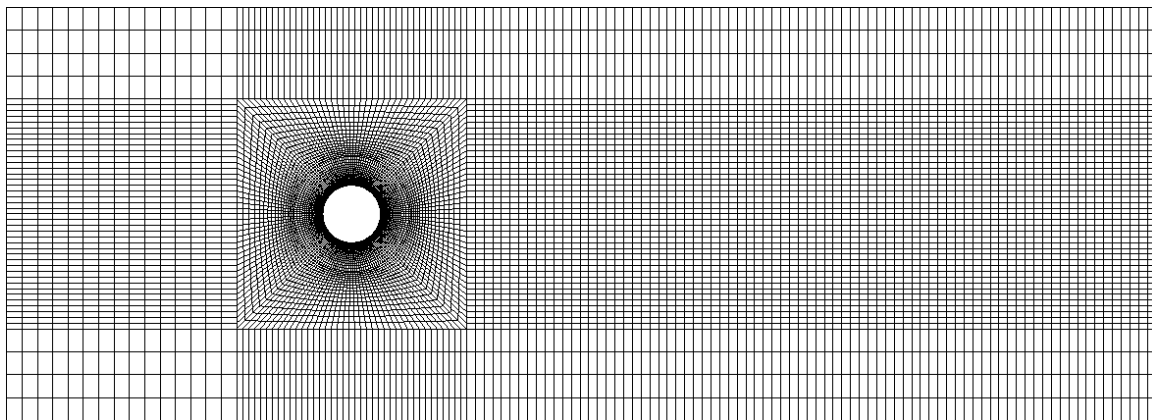


Fig. 4. Fine mesh in X-Y plane

The time step (normalized $\Delta T = tU/D$) used is 0.005 for the coarse mesh while for the fine mesh it is half of the one used for the coarse mesh. It takes roughly 4 to 5 sub-iterations for the unsteady residual to drop by two orders. A far-field boundary condition is used at the inlet with an unperturbed inlet flow velocity. At the outlet, a fixed pressure boundary condition is used. Periodic boundary condition is applied in the spanwise direction while symmetry is imposed for the top and bottom surfaces. Zero velocity boundary condition is used for the cylinder wall.

The flow over the cylinder is first allowed to reach a statistically steady state so as to allow all transients to exit the computational domain and then the statistics, mean and r.m.s. values, were obtained. The transients are convected out using 12 shedding periods and then 20 shedding periods are used to collect the statistics of mean and r.m.s. values.

IV. Numerical Results and Discussions

The instantaneous streamwise, transverse and spanwise velocities in the wake of the circular cylinder are shown in Fig. 5, 6 and 7. Fig 5 clearly shows the unsteady recirculation region. The alternating regions of positive and negative transverse velocity corresponding to the Karman vortices can also be observed in Fig. 6. At $Re_D=2580$, the flow becomes turbulent and three-dimensional which is evident of the presence of both the small and large scale structures in Fig. 7. It also shows that the flow structures increase in size as we go downstream of the cylinder. It can be noted that small scale structures are still present very far away from the cylinder which were not observed by Beaudan and Moin⁹. Moser *et al.*⁴⁰ performed a DNS and could capture the small scale and large scale turbulent structures at $Re_D=2000$.

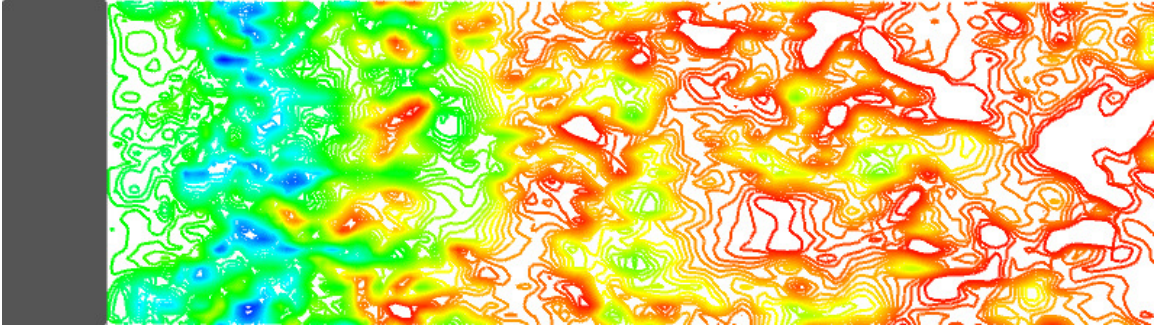


Fig. 5. Instantaneous streamwise velocity in x-z plane ($y=0$) in the wake of the cylinder. There are 40 contours from -0.1 to 0.1.

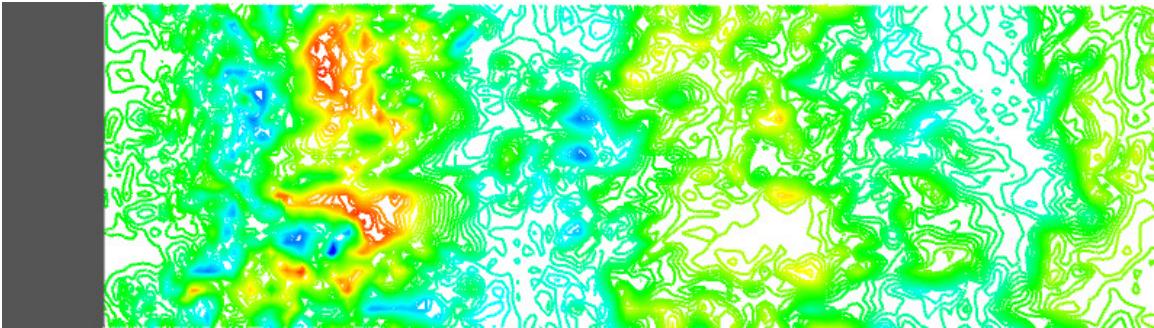


Fig. 6. Instantaneous transverse velocity in x-z plane ($y=0$) in the wake of the cylinder. There are 40 contours from -0.1 to 0.1.

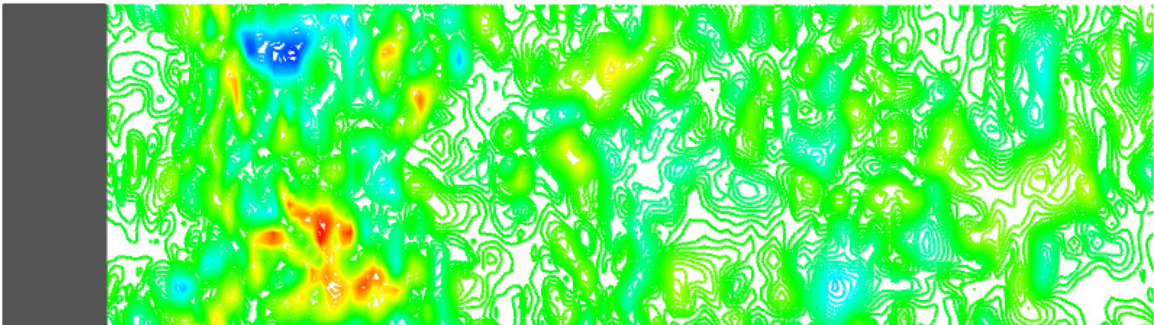


Fig. 7. Instantaneous spanwise velocity in x-z plane ($y=0$) in the wake of the cylinder. There are 52 contours from -0.1 to 0.1.

Fig. 8. shows contours of instantaneous vorticity magnitude. Two long shear layers can be seen separating from the cylinder. The Karman vortex street can also be seen in Fig. 8. The vortices arising from the instabilities of the shear layers mix in the primary Karman vortices before propagating downstream and similar observations were made by Chyu and Rockwell⁴¹ in their PIV experiments.

A study on grid independency is made for the coarse and fine mesh since insufficient grid resolution can lead to inaccurate predictions of the wake characteristics¹¹. Fig. 9 shows that the second order method cannot capture the statistics accurately. The coarse mesh with third order accuracy is in fairly good agreement with the experiment results. Fig. 10 and Fig. 11 show that both fine mesh and coarse mesh give excellent agreement with the experiment (PIV) measurements for the mean streamwise and transverse velocity at various locations in the wake of the cylinder. The fine mesh and coarse mesh results are pretty similar but the fine mesh gives slightly better results.

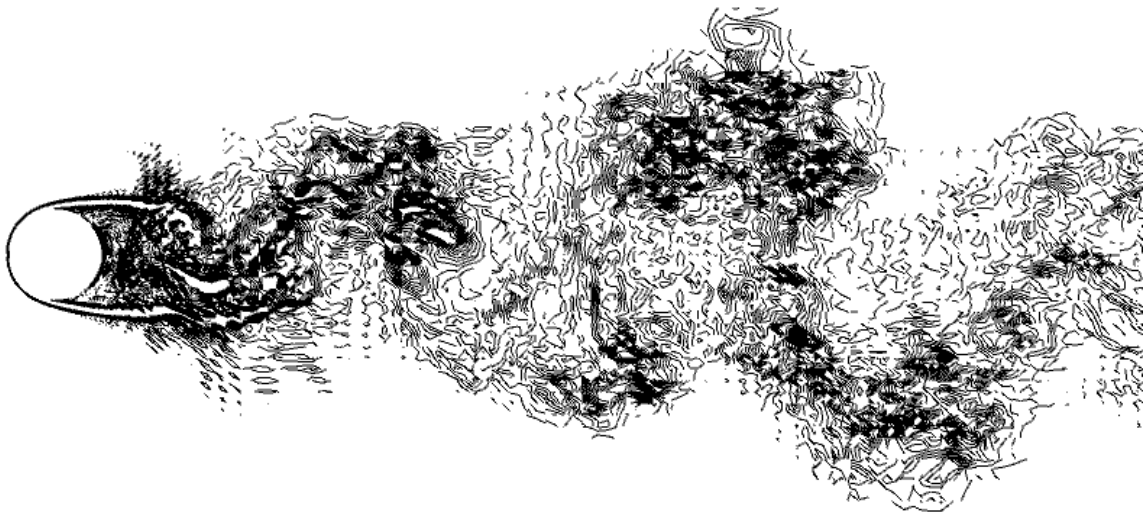


Fig. 8. Instantaneous vorticity magnitude showing 16 contours from $\omega D/U = -0.1$ to $\omega D/U = 0.1$.

At $x/D=1.5, 2$ and 2.5 , both the mean streamwise and transverse velocities are slightly over predicted for the coarse mesh. But the fine mesh results give a good agreement with the experiment values.

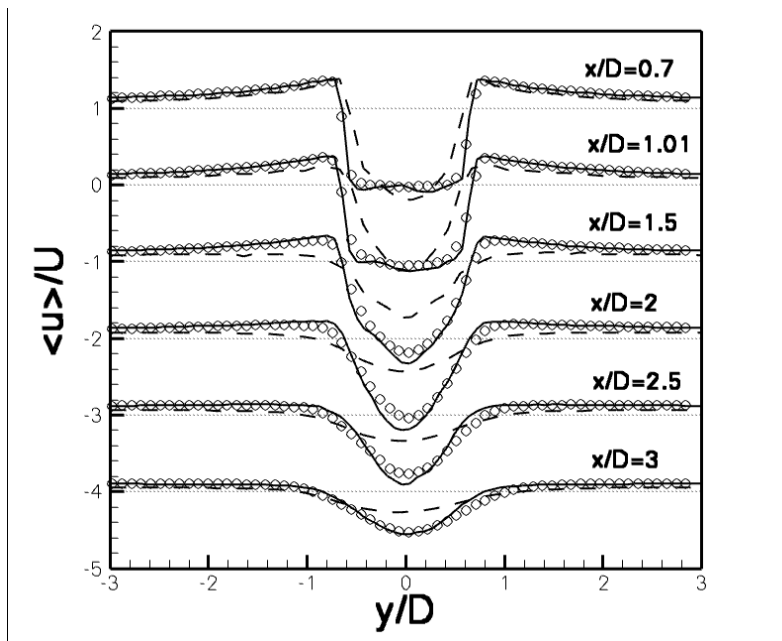


Fig. 9. Mean normalized streamwise velocity in the wake of the circular cylinder, (oooo) - experiment; (Dashed line) - 2nd order results; (Solid line) - 3rd order results. The dotted line (.....) represents the zero location of the shifted curves.

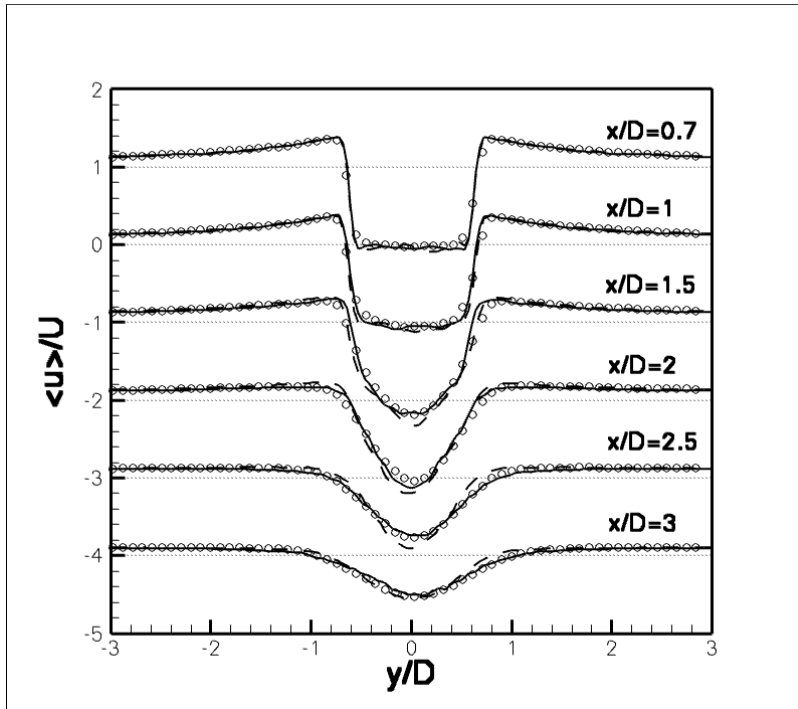


Fig. 10. Mean normalized streamwise velocity in the wake of the circular cylinder, (oooo) - experiment; (Dashed line) – coarse mesh; (Solid line) – fine mesh. The dotted line (.....) represents the zero location of the shifted curves.

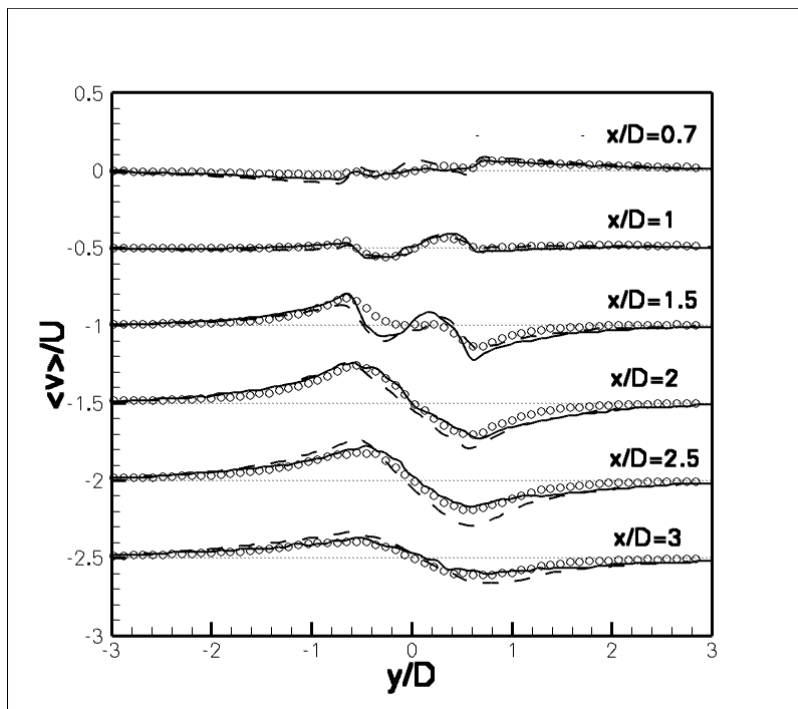


Fig. 11. Mean normalized transverse velocity in the wake of the circular cylinder, (oooo) - experiment; (Dashed line) – coarse mesh; (Solid line) – fine mesh. The dotted line (.....) represents the zero location of the shifted curves.

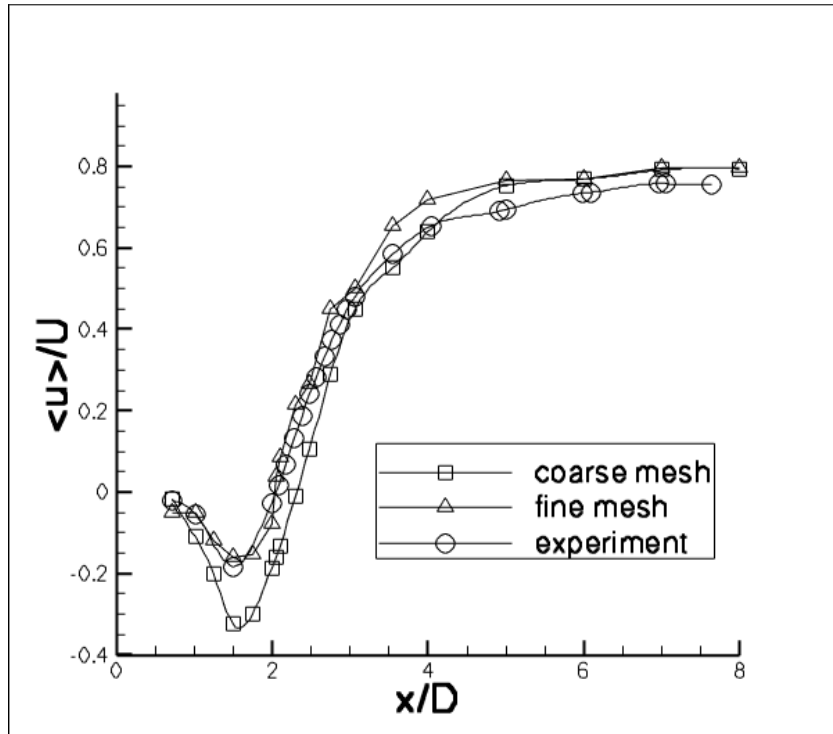


Fig. 12. Distribution of the streamwise mean velocity along the wake center-line.

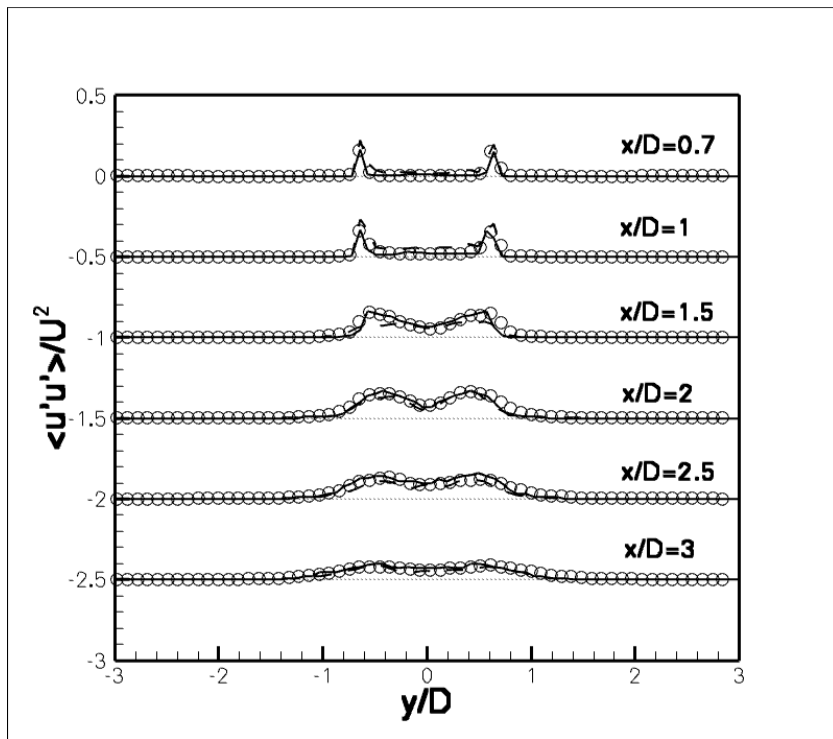


Fig. 13. Normalized $\langle u'u' \rangle / U^2$ in the wake of the circular cylinder, (oooo) - experiment; (Dashed line) – coarse mesh; (Solid line) – fine mesh. The dotted line (.....) represents the zero location of the shifted curves.

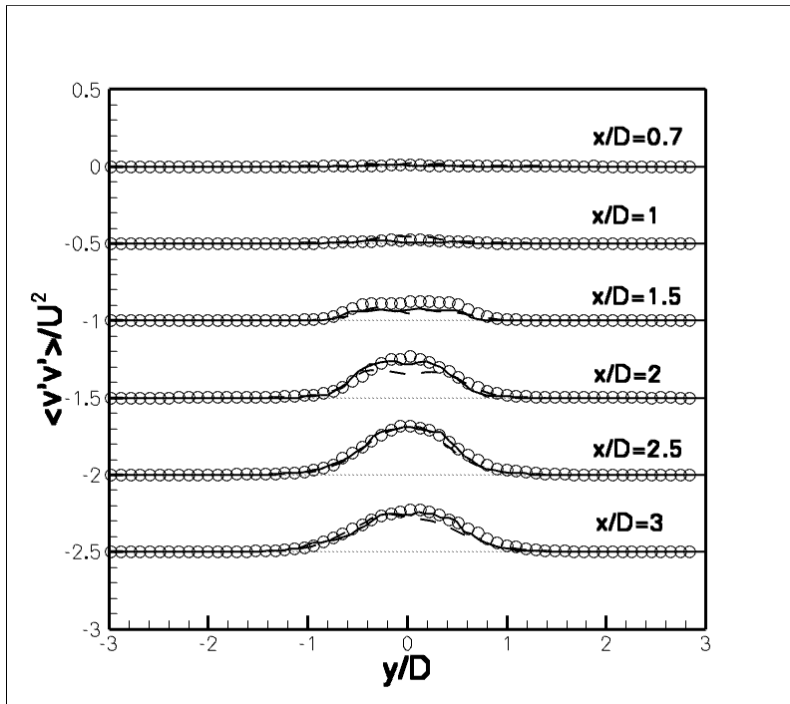


Fig. 14. Normalized $\langle v'v' \rangle / U^2$ in the wake of the circular cylinder, (oooo) - experiment; (Dashed line) – coarse mesh; (Solid line) – fine mesh. The dotted line (.....) represents the zero location of the shifted curves.

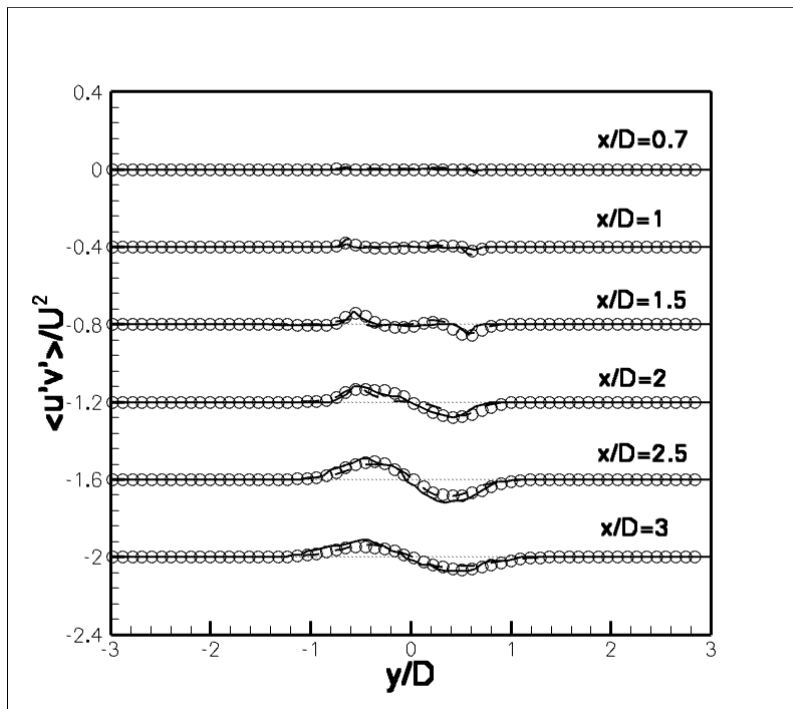


Fig. 15. Normalized $\langle u'v' \rangle / U^2$ in the wake of the circular cylinder, (oooo) - experiment; (Dashed line) – coarse mesh; (Solid line) – fine mesh. The dotted line (.....) represents the zero location of the shifted curves.

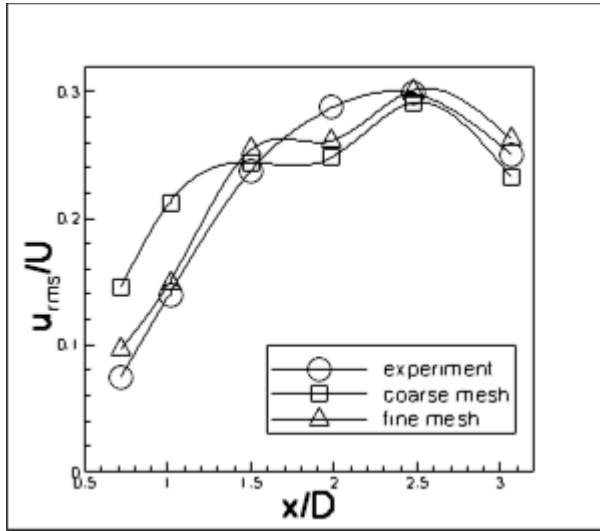


Fig. 16(a). Distribution of the streamwise r.m.s. velocities along the wake centerline.

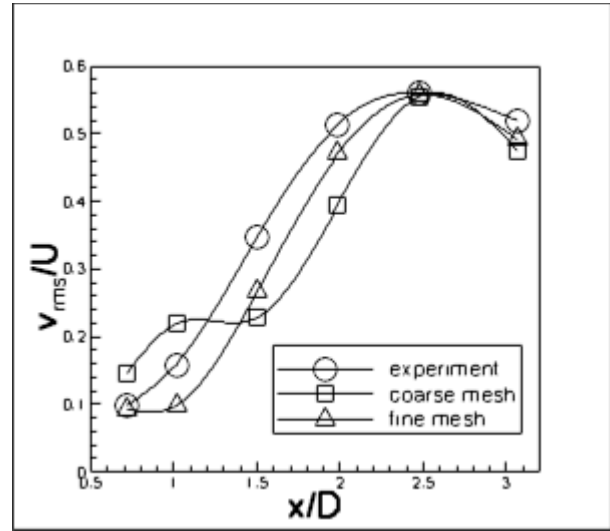


Fig. 16(b). Distribution of the transverse r.m.s. velocities along the wake centerline.

Fig. 12 shows the normalized streamwise mean velocity along the wake center-line. A small region of reversed flow occurs very near to the cylinder which is often defined as recirculation bubble. The velocity decreases and reaches a maximum negative value close to the cylinder and rises rapidly to positive values and finally reaching an asymptotic behavior far downstream. The length of the recirculation bubble is generally defined as the position downstream of the cylinder where the mean velocity becomes zero. The fine mesh gives an excellent agreement of the length of the recirculation bubble with the PIV measurements of Konstantinidis *et al.*²⁰. Though the coarse mesh does not predict the length of the recirculation bubble accurately, it gives a very good agreement of mean velocity at the wake center line further downstream.

Fig. 13 and Fig. 14 show respectively the normalized time-averaged streamwise and cross-wake Reynolds stresses. The peaks in the streamwise Reynolds stress are predicted very well. But the cross-stream Reynolds stress is a little under predicted at $x/D=1.5$. The shear stress predictions are shown in Fig. 15. Both the coarse mesh and fine mesh are in good agreement with the experiment.

The distribution of the normalized streamwise and transverse r.m.s. velocities along the wake center line is shown in Fig. 16 (a) and (b). Fig. 16(a) shows a peak at a position which is a measure of vortex formation length (Griffin⁴²). Similar peak is observed in the case of transverse r.m.s. velocity distribution along the wake center line. It can be noted from Fig. 16 (a) and 16 (b) that the magnitude of the transverse fluctuations is roughly two times that of the streamwise fluctuations at almost every position due to the way that vortices are formed, typical of bluff body wakes. The maximum r.m.s. fluctuations along the wake center line for the fine mesh is in good agreement with the experiment results. The maximum streamwise r.m.s. velocity $(u/U)_{\max}$ for the coarse mesh is slightly less than the experiment results. The maximum values were over predicted by Konstantinidis *et al.*⁴³. The results agree very well with the ones published by Noberg⁴⁴ at a slightly higher Reynolds number $Re_D=3000$.

V. Conclusion

Uniform flow past a circular cylinder at a Reynolds number of $Re_D=2580$ was simulated using the spectral difference method. The predictions for the mean velocities and Reynolds stresses agree well with the experiment results obtained by Konstantinidis *et al.*²⁰. The second order results are inaccurate but higher order ($=3$) of spatial accuracy gives excellent results. The length of the recirculation bubble and vortex formation length were very well predicted. The effect of mesh refinement was also studied by considering both coarse and fine meshes. Higher order results on a finer mesh showed the best agreement with experimental data. The wake characteristics were very well captured with the third order SD method, demonstrating its effectiveness and potential in handling bluff body problems and vortex dominated flows.

Acknowledgements

This study has been supported by the Air Force Office of Scientific Research (AFOSR) grant FA9550-06-1-0146, and the Department of Energy (DOE) grant DE-FG02-05ER25677. The views and conclusions contained herein are those of the authors and should not be interpreted as necessarily representing the official policies or endorsements, either expressed or implied, of the AFOSR and DOE.

References

1. C. H. K. Williamson, R. Govardhan, "Vortex induced vibrations", *Annual Review of Fluid Mechanics*, Vol. 36, 2004, pp. 413-455.
2. T. Sarpkaya, "A critical review of the intrinsic nature of vortex-induced vibrations", *Journal of Fluids and Structures*, Vol. 19, 2004, pp. 389-447.
3. C. H. K. Williamson, "Vortex dynamics in the cylinder wake", *Annual Review of Fluid Mechanics*, Vol. 28, 1996, pp. 477-539.
4. A. Travin, M. Shur, M. Strelets, P. Spalart, "Detached-eddy simulations past a circular cylinder", *Flow, Turbulence and Combustion*, Vol. 63, 1999, pp. 293-313.
5. P. Catalano, M. Wang, G. Lacarino, P. Moin, "Numerical simulation of the flow around a circular cylinder at high Reynolds numbers", *International Journal of Heat and Fluid Flow*, Vol. 24, 2003, pp. 463-469.
6. M. Laurenci, C. Shih, "Characteristics of the plane turbulent near wake of a circular cylinder, a particle image velocimetry study", *Private communication by Beaudan and Moin*, 1993.
7. L. Ong, J. Wallace, "The velocity field of the turbulent very near wake of a circular cylinder", *Exp. Fluids*, Vol. 20, 1996, pp. 441-453.
8. Michael Breuer, "Numerical and modeling influences on large eddy simulations for the flow past a circular cylinder", *International Journal of Heat and Fluid Flow*, Vol. 19, 1998, pp. 512-521.
9. P. Beaudan, P. Moin, "Numerical experiments on the flow past a circular cylinder at a subcritical Reynolds number", *Technical report TF-62, Thermosciences Division, Department of Mechanical Engineering, Stanford University*, 1994.
10. R. Mittal, P. Moin, "Suitability of upwind-biased finite-difference schemes for large-eddy simulation of turbulent flow", *AIAA Journal*, Vol. 35, 1997, pp. 1415-8.
11. A. G. Kravchenko, P. Moin, "Numerical studies of flow over a circular cylinder at $Re_D=3900$ ", *Physics of Fluids*, Vol. 12, 2000, pp. 403-417.
12. J. Frohlich, W. Rodi, P. Kessler, J. P. Bertoglio, D. Laurence, "Large eddy simulation of flow around circular cylinder on structured and unstructured grids", *In: E. H. Hirshel, editor. Notes on numerical fluid mechanics*, Vol. 66, 1998, pp. 319- 338.
13. X. Ma, G. S. Karamanos, G. E. Karniadakis, "Dynamics and low dimensionality of a turbulent near wake", *Journal of Fluid Mechanics*, Vol. 410, 2000, pp. 29-65.
14. R. P. Hasen, L. N. Long, "Large eddy simulation of a circular cylinder on unstructured grids", *AIAA Paper 2002-0982*.
15. A. G. Kravchenko, P. Moin, "B-spline methods and zonal grids for numerical simulations of turbulent flows", *Technical report TF-73, Department of Mechanical Engineering, Stanford University, USA*, 1998.
16. M. M. Rai, P. Moin, "Direct numerical simulation of transition and turbulence in a spatially evolving boundary layer", *Journal of Computational Physics*, Vol. 109, 1993, pp. 169.
17. Michael Breuer, "Large eddy simulation of the subcritical flow past a circular cylinder: numerical and modeling aspects", *International Journal for Numerical Methods in Fluids*, Vol. 28, 1998, pp. 1281-1302.
18. J. Franke, W. Frank, "Large eddy simulation of the flow past a circular cylinder at $Re_D=3900$ ", *Journal of Wind Engineering and Industrial Aerodynamics*, Vol. 90, 2002, pp. 1191-1206.
19. C. Liang, G. Papadakis, "Large eddy simulation of pulsating flow over a circular cylinder at subcritical Reynolds number", *Computers and Fluids*, Vol. 36, n 2, February 2007, pp. 299-312.
20. E. Konstantinidis, S. Balabani, M. Yianneskis "Conditional averaging of PIV plane wake data using a cross-correlation approach", *Experiments in Fluids*, Vol. 39, 2005, pp. 38-47.
21. Y. Liu, M. Vinokur, Z. J. Wang, "Discontinuous Spectral Difference Method for Conservation laws on unstructured grids", *In proceedings of the 3rd International Conference in CFD, Toronto, Canada*, July 2004.

22. Y. Liu, M. Vinokur, Z. J. Wang, "Multi-dimensional Spectral Difference method for unstructured grids", *AIAA-2005-0320*.
23. Z. J. Wang, Y. Liu, "The Spectral Difference method for the 2D Euler equations on unstructured grids", *AIAA-2005-5112*.
24. P. G. Huang, Z. J. Wang, Y. Liu, "An Implicit space-time Spectral Difference method for discontinuity capturing using adaptive polynomials", *AIAA-2005-5255*.
25. B. Cockburn, C. W. Shu, "TVB Runge-Kutta local projection discontinuous Galerkin finite element method for conservation laws II: General framework", *Math. Comput.*, Vol. 52, 1989, pp. 411.
26. B. Cockburn, C. W. Shu, "The Runge-Kutta discontinuous Galerkin method for conservation laws V: multidimensional systems", *Journal of Computational Physics*, Vol. 141, 1998, pp. 199-224.
27. Z. J. Wang, Liu Yen, "Spectral (Finite) Volume Method for Conservation Laws on Unstructured Grids III: Extension to One-Dimensional Systems", *Journal of Scientific Computing*, Vol. 20, No. 1, 2004, pp. 137-157.
28. Z. J. Wang, L. Zhang, Y. Liu, "Spectral (Finite) Volume method for conservation laws on unstructured grids IV: extension to two-dimensional systems", *Journal of Computational Physics*, Vol. 194, 2004, pp. 716-741.
29. Y. Liu, M. Vinokur, Z. J. Wang, "Spectral (Finite) Volume Method for Conservation Laws on Unstructured Grids V: Extension to Three-Dimensional Systems", *Journal of Computational Physics*, Vol. 212, 2006, pp. 454-472.
30. Y. Sun, Z. J. Wang, Y. Liu, "Spectral (Finite) Volume Method for Conservation Laws on Unstructured Grids VI: Extension to Viscous Flow", *Journal of Computational Physics*, Vol. 215, No.1, 2006, pp. 41-58.
31. Y. Sun, Z.J. Wang and Y. Liu, "High-Order Multidomain Spectral Difference Method for the Navier-Stokes Equations on Unstructured Hexahedral Grids", *Communications in Computational Physics*, Vol. 2, No. 2, pp. 310-333, 2007.
32. Y. Sun, Z.J. Wang and Y. Liu, "Efficient Implicit Non-linear LU-SGS Approach for Compressible Flow Computation Using High-Order Spectral Difference Method", *Communications in Computational Physics*, Vol. 5, No. 2-4, pp. 760-778, 2009.
33. D.A. Kopriva, A Staggered-Grid Multidomain Spectral Method for the Compressible Navier-Stokes Equations, *Journal of Computational Physics*, Volume 143, pp. 125-158, 1998.
34. K Van den Abeele, C. Lacor and Z.J. Wang, "On the stability and accuracy of the spectral difference method," *Journal of Scientific Computing*, in press.
35. H.T., Huynh, "A Flux Reconstruction Approach to High-Order Schemes Including Discontinuous Galerkin Methods," *AIAA-2007-4079*.
36. H. Mansy, P. M. Yang, D. R. Williams, "Quantitative measurements of three-dimensional structures in the wake of a circular cylinder", *J. of fluid mechanics*, Vol. 270, 1994, pp. 227.
37. C. H. K. Williamson, J. Wu, J. Sheridan, "Scaling of streamwise vortices in wakes", *Physics of Fluids*, Vol. 7, 1995, pp. 2307.
38. S. Yoon and A. Jameson A, "Lower-upper symmetric-Gauss-Seidel method for the Euler and Navier-Stokes equations", *AIAA Journal*, 1988, Vol. 26, pp. 1025-1026.
39. R.F. Chen, and Z.J. Wang, "Fast, Block Lower-Upper Symmetric Gauss-Seidel Scheme for Arbitrary Grids", *AIAA Journal*, 2000, Vol. 38, no. 12, pp. 2238-2245.
40. R. D. Moser, M. M. Rogers, D. W. Ewing, "Self-similarity of time evolving plane wakes", *Journal of Fluid Mechanics*, Vol. 367, 1998, pp. 255-289.
41. C. K. Chyu, D. Rockwell, "Near wake structure of an oscillating cylinder: Effect of controlled shear layer vortices", *Journal of Fluid Mechanics*, Vol. 322, 1996, pp. 21-49.
42. O. M. Griffin, "A note on bluff body vortex formation", *Journal of Fluid Mechanics*, Vol. 284, 1995, pp. 217-224.
43. E. Konstantinidis, S. Balabani, M. Yianneskis, "The effect of flow perturbations on the near wake characteristics of a circular cylinder", *Journal of Fluids and Structures*, Vol. 18, 2003, pp. 367-386.
44. C. Noberg, "Interaction of free stream turbulence and vortex shedding for a single tube in cross-flow", *Journal of Wind Engineering and Industrial Aerodynamics*, Vol. 23, 1986, pp. 501-514.